ORGANOMETALLICS

Article

Cite This: *Organometallics* XXXX, XXX, XXX–XXX

Iron(II)-Catalyzed Hydrogenation of Acetophenone with a Chiral, Pyridine-Based PNP Pincer Ligand: Support for an Outer-Sphere Mechanism

Raffael Huber, Alessandro Passera, and Antonio Mezzetti*

Department of Chemistry and Applied Biosciences, ETH Zurich, Zurich 8093, Switzerland

Supporting Information

ABSTRACT: We report here the tridentate, P-stereogenic, C_2-symmetric PNP pincer ligand (S_P,S_P)-2,6-bis((cyclohexyl-(methyl)phosphanyl)methyl)pyridine (**1a**) and its iron(II) complexes [$FeBr_2$(CO)(**1a**)] (**2a**), [FeHBr(CO)(**1a**)] (**3a**), and [FeH_2(CO)(**1a**)] (**4a**). In the presence of base, bromocarbonylhydride **3a** catalyzes the hydrogenation of acetophenone to (*S*)-1-phenylethanol with 48% ee. The transition states of the enantiodetermining transfer of hydride from **3a** to the carbonyl group of acetophenone were studied by density functional theory (DFT) with a full conformational analysis of the PNP ligand for the three different mechanistic models recently proposed for a related achiral catalyst. The DFT calculations show that the outer-sphere monohydride mechanism originally proposed by Milstein reproduces the experimentally observed sense of induction (*S*) and enantioselectivity, whereas the dihydride and inner-sphere pathways predict the formation of the *R* enantiomer.

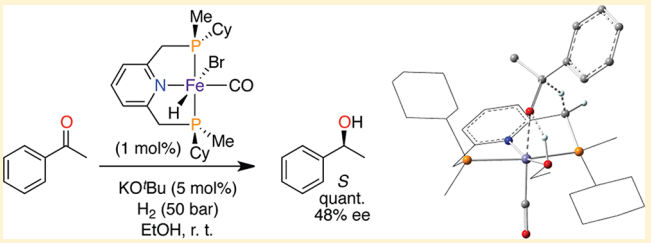

INTRODUCTION

Since Casey's and Guan's seminal report of the first well-defined iron catalyst for the hydrogenation of ketones,[1] several iron(II) catalysts have been developed for the asymmetric hydrogenation of polar double bonds.[2] Its enantioselective version is one of the most important catalytic reactions in industry,[3] and two chiral ligand platforms play a major role with iron(II). Tetradentate N_2P_2 ligands, either linear[4] or macrocyclic,[5,6] efficiently catalyze the asymmetric transfer hydrogenation (ATH) of polar double bonds, whereas PNP pincers are the ligands of choice in the asymmetric direct (H_2) hydrogenation (AH, Chart 1).[7] Thus, complexes of the type

Chart 1. Selection of Iron Catalysts for Asymmetric Direct Hydrogenation

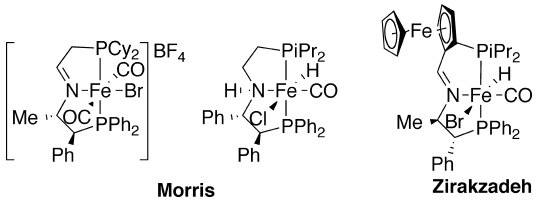

[FeHBr(CO)(PNP)] (where PNP is a chiral pincer ligand with an NP_2 donor set) have found successful application in the asymmetric direct hydrogenation of ketones.[8] Morris prepared chiral PNP pincers based on a disubstituted 2-phosphinoethylamine,[8a,c] and Zirakzadeh introduced a ferrocenyl link between the amine and a phosphine as further stereogenic element (Chart 1).[8b]

In contrast to backbone-based chirality, stereogenic P atoms—which are recognized as powerful units to impart enantioselectivity in catalytic processes[9]—are still virtually unexplored with pincer ligands.[10] An achiral scaffold that can be readily modified to a chiral, P-stereogenic PNP pincer is 2,6-dimethylenepyridine. Milstein has used achiral PNP pincer ligands such as **1b** (Chart 2) in the iron-catalyzed hydro-

Chart 2. PNP Ligands and [$FeBr_2$(CO)(PNP)] Complexes

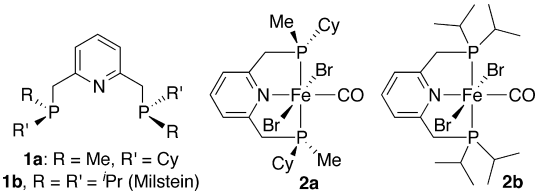

genation of ketones,[11] esters,[12] aldehydes,[13] and amides.[14] In view of these remarkable results, we decided to prepare chiral, C_2-symmetric PNP ligands such as **1a** in Chart 2 and to study their Fe(II) complexes as catalysts for the asymmetric direct hydrogenation of ketones.

During the development of this project, we realized that a chiral PNP ligand based on the 2,6-dimethylenepyridine backbone may help disentangle the controversy concerning the mechanism of ketone hydrogenation with their iron(II) complexes. In fact, three different mechanism types have been

Received: November 9, 2017

DOI: 10.1021/acs.organomet.7b00816
Organometallics XXXX, XXX, XXX–XXX

proposed for the direct hydrogenation of ketones with the achiral bromocarbonylhydride [FeHBr(CO)(**1b**)] (**3b**) using density functional theory (DFT) calculations (Chart 3).[15−17]

Chart 3. Proposed Transition States for the Direct Hydrogenation of Acetophenone with Catalyst 3b

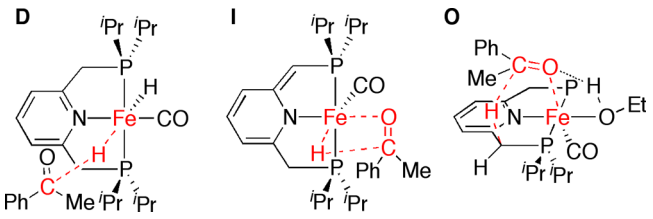

The first suggestion,[16] which has been recently revised,[17] is the outer-sphere mechanism **D** based on the dihydride complex [FeH_2(CO)(**1b**)] (**4b**) as catalytically active species. Alternatively, Milstein considered an inner-sphere mechanism involving hydride transfer from a complex bearing a deprotonated PNP ligand (**I**).[11] This mechanism was later discarded because of its unrealistically high calculated energetic span[18] (50.8 kcal mol^{-1}), and an unprecedented outer-sphere mechanism was put forward in which an iron(0) complex transfers a benzylic H atom of the PNP ligand as hydride to acetophenone (**O**).[15] The much lower energetic span of **O** (21.7/24.5 kcal mol^{-1}) compared to that of **I** and the observation that dihydride **4b** is unreactive toward acetophenone make **O** the most likely mechanism.[15]

As the use of a chiral catalyst introduces additional stereochemical information, we wondered whether the enantioselectivity and sense of chiral induction observed experimentally and those estimated by DFT calculations may allow discriminating between mechanisms **I**, **O**, and **D**. Therefore, we prepared the P-stereogenic PNP pincer ligand **1a** and its mono- and dihydride complexes and tested them as catalysts in the asymmetric hydrogenation of ketones. Parallel to this, we studied the transition states of the enantiodetermining hydride transfer to the carbonyl group of acetophenone by DFT with the three mechanistic models recently proposed for the related achiral catalyst **2b**.[15−17] The results of this combined experimental and DFT study are reported below.

RESULTS AND DISCUSSION

Synthesis of the Pincer Ligand. As a chiral analogue of **1b**, we prepared the pincer ligand (S_P,S_P)-2,6-bis((cyclohexyl(methyl)phosphanyl)methyl)pyridine (**1a**) by alkylation of 2,6-bis(chloromethyl)pyridine with (*S*)-cyclohexylmethylphosphine borane **5** (Scheme 1).

Scheme 1. Synthons for Pincer Ligand 1a

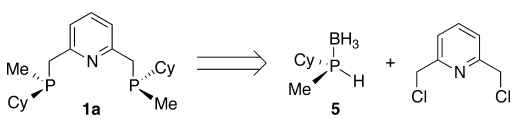

The key synthon for **1a** is (*S*)-cyclohexylmethylphosphine borane (**5**, Scheme 1). Enantiomerically pure cyclohexylmethylphosphine borane **5** has been previously prepared by separation of the diastereomers of bornylthio(cyclohexyl)methylphosphine borane by preparative HPLC.[19] In our stereoselective approach, (*R*)-cyclohexyl(hydroxylmethyl)methylphosphine borane (**7**) was prepared by enantioselective deprotonation of cyclohexyldimethylphosphine borane (**6**) with (−)-sparteine and *sec*-butyllithium, followed by O_2 oxidation (Scheme 2).[20,21]

Scheme 2. Synthesis of (*R*)-Cyclohexyl(hydroxymethyl)methylphosphine Borane 7

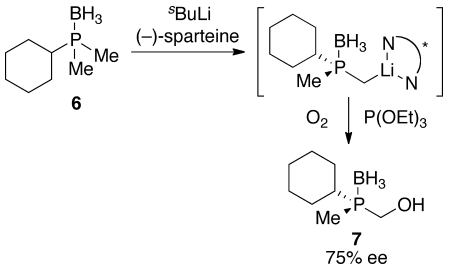

Crude hydroxymethylphosphine borane **7** was isolated as an oil in 75% ee, and its enantiomeric purity was improved by esterification with *p*-phenylbenzoyl chloride to (boranyl(cyclohexyl)(methyl)phosphanyl)methyl[1,1′-biphenyl]-4-carboxylate (**8**, Scheme 3).[22] This highly crystalline ester was recrystallized from ethyl acetate/hexane until it was optically pure, which typically required two crystallizations steps. After hydrolysis and oxidation−decarboxylation,[21] the secondary phosphine borane **5** was obtained with 99.6% ee in 44% yield over three steps.

Scheme 3. Synthesis of Enantiomerically Pure Secondary Phosphine Borane 5

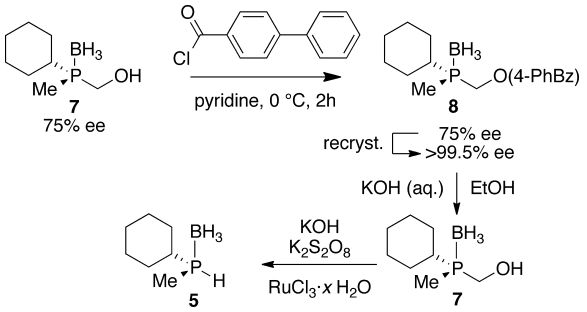

The secondary phosphine borane **5** was deprotonated with ^{n}BuLi, and addition of 2,6-bis(chloromethyl)pyridine gave the borane-protected pincer ligand **9a** in high yield (90%) (Scheme 4).

[$FeBr_2$(CO)(PNP)]. Phosphine borane **9a** was deprotected with HBF_4·OEt_2 in dichloromethane (Scheme 5).[23,24] Treatment of the free ligand **1a** with $FeBr_2$ under a CO atmosphere (1.1 atm) gave the deep blue dibromocarbonyl complex [$FeBr_2$(CO)(**1a**)] (**2a**), which was precipitated with pentane, filtered off in air, and purified by washing with water, ethanol,

Scheme 4. Preparation of Borane-Protected PNP Pincer Ligand 9a

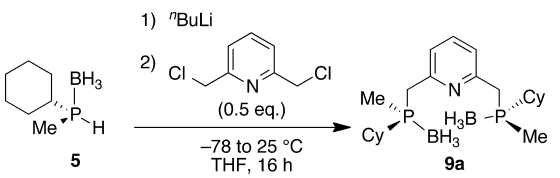

DOI: 10.1021/acs.organomet.7b00816
Organometallics XXXX, XXX, XXX−XXX

Scheme 5. Preparation of Dibromocarbonyl Complex 2a

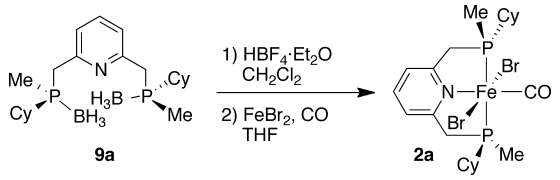

diethyl ether, and pentane. The $^{31}P\{^{1}H\}$ NMR spectrum of **2a** shows a singlet at δ 59.6, indicating a C_2-symmetric complex and hence mutually *trans*-bromido ligands. A trace amount of its *cis*-isomer is also present (δ 52.2 and 42.9, $^{2}J_{P,P'}$ = 203.3 Hz, <2%).

Complex **2a** is perfectly stable toward air and moisture both in solution and in the solid state. No decomposition was observed after storing solid samples thereof in air at room temperature for several months. In solution, **2a** is stable for at least 2 weeks without precautions to exclude air or moisture. The IR spectrum shows a CO band at 1945 cm^{-1} (**2a**), which indicates that the π-basicity of the iron(II) center in **2a** is very similar to that in the achiral [$FeBr_2$(CO)(**1b**)] analogue **2b** (ν_{CO} = 1944 cm^{-1}).[11] X-ray quality crystals of **2a** were obtained by slow diffusion of pentane into a THF solution. Complex **2a** displays a slightly distorted octahedral geometry with mutually *trans*-bromides (Figure 1).

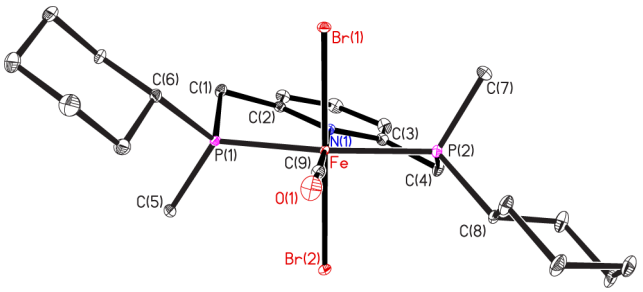

Figure 1. ORTEP drawing of **2a** (ellipsoids at 30% probability). Selected bond lengths (Å) and (torsion) angles (deg): Fe–P(1), 2.2313(8); Fe–P(2), 2.2414(8); Fe–N(1), 2.042(2); Fe–C(9), 1.744(3); Fe–Br(1), 2.4533(5); Br(1)–Fe–P(1), 86.68(2); Br(1)–Fe–P(2), 91.67(3); P(1)–Fe–N(1)–C(2), 14.3(2); P(2)–Fe–N(1)–C(3), 16.2(2).

The most striking difference between the chiral **2a** and achiral [$FeBr_2$(CO)(**1b**)] (**2b**) are the Fe–P bond lengths, which are considerably shorter in **2a** (2.2313(8), 2.2414(8) Å) than in **2b** (2.3020(14), 2.2799(14) Å).[11] We attribute this to the lower steric bulk of cyclohexylmethylphosphine in comparison with that of diisopropylphosphine. In **2b**, the repulsion between the isopropyl substituent and bromide leads to an obtuse Br(1)–Fe–P(2) angle of 94.35(4)°. This distortion is less pronounced in **2a** (91.67(3)°).

[FeHBr(CO)(PNP)]. Bromohydridocarbonyl complex **3a** was obtained by treatment of dibromocarbonyl **2a** with $NaBHEt_3$ (1 equiv) in THF at room temperature for 4 h (Scheme 6). Evaporation of the solvent and washing with pentane gave a brown solid that was dried, stored under argon at −20 °C, and characterized by NMR and IR spectroscopy. The $^{31}P\{^{1}H\}$ NMR spectrum of the reaction solution of **2a** shows a mixture of products. The major one is a hydride complex featuring a ^{1}H NMR signal at δ −20.95 (dd, $^{2}J_{P,H}$ = 56.6, 50.9 Hz) and a ^{31}P NMR AX system at δ 76.1 and 64.9 (d, $^{2}J_{P,P'}$ = 139.0 Hz) (as

Scheme 6. Preparation of Bromocarbonylhydride 3a

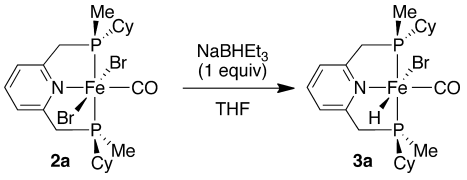

determined by $^{31}P-^{1}H$ correlation spectroscopy). We formulate this species as [FeHBr(CO)(**1a**)] (**3a**), in which H is *trans* to Br (Scheme 6) in analogy to Milstein's [FeHBr(CO)(**1b**)] (**3b**).[11] A minor ^{31}P NMR AX system (δ = 72.9 and 65.0, $^{2}J_{P,P'}$ = 159.9 Hz, 15%) that correlates to a ^{1}H NMR signal at δ −22.0 (dd, $^{2}J_{P,H}$ = 55.7, 49.6 Hz) is assigned to the isomer of **3a** with hydride *trans* to the pyridine nitrogen, as a hydride ligand *trans* to CO would give a ^{1}H NMR signal at a much higher frequency.[25] Finally, a ^{31}P NMR singlet at δ 82.9 (12%) probably corresponds to a dicarbonyl Fe(0) complex, which has already been observed as a decomposition product in the case of **3b**.[11] The presence of the latter complex as an impurity may explain the poor elemental analysis of **3a**. Attempts to further purify the iron hydride **3a** failed as it slowly decomposes in solution. Upon prolonged (>1 month) storage of a C_6D_6 solution of **3a**, some decomposition products in the form of a brown precipitate are observed. The signals of both hydride complexes have disappeared, and the ^{31}P NMR spectrum shows only the signals of the putative dicarbonyl complex (at δ 83.4) and of dibromocarbonyl **2a**.

The CO stretch of **3a** (1902 cm^{-1}) is red-shifted with respect to dibromocarbonyl **2a** (1945 cm^{-1}), as expected for the more electron-rich hydride complex, in which π-backbonding to CO is increased. The CO band of **3a** also displays a shoulder at 1850 cm^{-1}, which might be assigned to the ν_{Fe-H} stretching or, alternatively, to the putative dicarbonyl impurity. Hydride **3a** is stable when stored as solid under argon at −20 °C in the absence of light but is highly air-sensitive in solution. Exposure of CD_2Cl_2 solutions to air leads to an immediate color change from green to yellow, and a brown, unidentified precipitate is formed.

[FeH_2(CO)(1a)]. Dihydride **4a** was prepared by treating dibromocarbonyl **2a** with $NaHBEt_3$ (2.1 equiv) in THF (Scheme 7). The addition of the hydride source was

Scheme 7. Preparation of Carbonyldihydride 4a

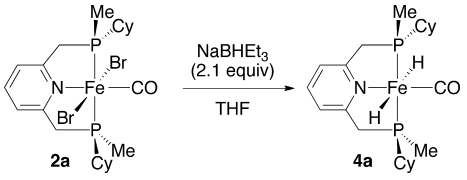

accompanied by an immediate color change from deep blue to brownish-yellow. After evaporation of the volatiles, the complex was extracted with diethyl ether to give a yellow solution, which was filtered and evaporated to dryness.

The resulting brown-yellow product contained a mixture of products. The major hydride species (93% of total intensity) shows a characteristic signal at δ −7.65 (t, $^{2}J_{P,H}$ = 41.5 Hz) and a broad ^{31}P NMR triplet at δ 86.4 ($^{2}J_{P,H}$ = 41.5 Hz), as confirmed by $^{31}P-^{1}H$ correlation spectroscopy, and is formulated as *trans*-[FeH_2(CO)(**1a**)] (**4a**) based on the C_2-symmetry of the complex. Accordingly, *trans*-[FeH_2(CO)(**1b**)]

DOI: 10.1021/acs.organomet.7b00816
Organometallics XXXX, XXX, XXX–XXX

(**4b**) has a hydride chemical shift of δ −7.27.[15] A minor, unidentified, C_1-symmetric hydride (7%) gives an apparent ^{1}H NMR triplet at δ −9.91 ($^2J_{P,H}$ = 49.6 Hz) and an AX system in the ^{31}P{^{1}H} NMR spectrum at δ 80.0 and 69.6 ($^2J_{P,P'}$ = 139.2 Hz). Attempts to obtain a pure product failed, as **4a** is soluble even in alkanes and slowly decomposes in solution.

Addition of a stoichiometric amount of acetophenone to a C_6D_6 solution of this mixture did not lead to a change in the hydride region of the ^{1}H NMR spectrum, with the species at δ = −7.65 still present as the major signal after 24 h. In the ^{31}P{^{1}H} NMR spectrum, trace amounts (<3%) of a new AX system at δ = 84.2 and 74.9 (d, $^2J_{P,P'}$ = 30.4 Hz) appeared. ^{31}P−^{1}H correlation spectroscopy shows that this species is not a hydride complex. After hydrolysis, GC-MS analysis revealed that trace amounts (<2%) of phenylethanol were formed, which may originate from an impurity in the dihydride complex, though, because the major *trans*-dihydride does not react. We conclude that dihydride **4a** is not a reactive intermediate in catalysis—as previously observed by Milstein for its achiral analogue [FeH_2(CO)(**1b**)] (**4b**).[15]

When the isomeric mixture of dihydride **4a** was dissolved in ethanol-d_6, a red solution was obtained, whose ^{1}H NMR spectrum showed no hydride resonance. Upon addition of KO^{t}Bu (1 equiv), the color of the solution changed immediately to yellow, but no hydride signal was visible by ^{1}H NMR spectroscopy. Therefore, in both cases, putative hydride-containing species are either absent (due to decomposition) or, less probably, paramagnetic.

Asymmetric Hydrogenation of Acetophenone. The reaction conditions in the direct hydrogenation of acetophenone (**10**) to 1-phenylethanol (**11**) were optimized for catalyst **3a**. Starting from similar reaction conditions (EtOH, 20 °C, 5 bar H_2) as used for the achiral analogue [FeHBr(CO)(**1b**)] (**3b**) (Scheme 8),[11] quantitative acetophenone conversion was

Scheme 8. Asymmetric Hydrogenation of 10 with 3a

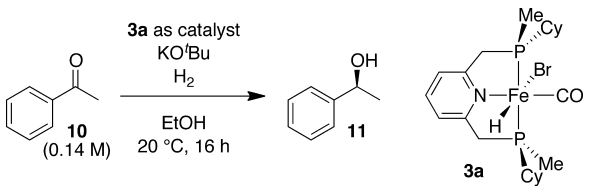

achieved at 50 bar H_2 (Table 1, entry 3). Catalyst loadings lower than 1 mol % (entries 4 and 5) led to lower conversion, in contrast to Milstein's achiral analogue [FeHBr(CO)(**1b**)] (**3b**), which operates at catalyst loadings as low as 0.05 mol %.[11] As observed with **3b**,[11] ethanol is the solvent of choice for the reaction. Catalyst **3a** is less active in ^{n}PrOH and ^{n}BuOH (with no effect on the enantioselectivity, entries 8 and 9), poorly active in MeOH (entry 7), and inactive in THF (entry 10).

Generating the hydride complex **3a** in situ from **2a** gave results almost identical to those of the isolated complex (entry 3 vs 6), which is more convenient in view of the easy handling of the dibromocarbonyl precursors. Under optimized conditions, the isolated hydride **3a** gave quantitative conversion and 48% ee under 50 bar of H_2 pressure (entry 3). Addition of PMe_3 as a poisoning agent for Fe nanoparticles[4c] to a catalytic run with **3a** did not alter the reaction outcome, which indicates that the catalyst remains homogeneous under reaction conditions (entry 11). An investigation of the substrate scope

Table 1. Optimization of the Hydrogenation of 10[a]

entry	cat.	S/C/B	solvent	$p(H_2)$ (bar)	conv.[b] (%)	ee[b] (%)
1	**3a**	100/1/5	EtOH	5	6	nd
2	**3a**	100/1/5	EtOH	20	65	48
3	**3a**	100/1/5	EtOH	50	quant.	48
4	**3a**	200/1/5	EtOH	50	22	48
5	**3a**	1000/1/5	EtOH	50	15	49
6[c]	**3a**	100/1/5	EtOH	50	quant.	46
7	**3a**	100/1/5	MeOH	50	4	nd
8	**3a**	100/1/5	^{n}PrOH	50	54	48
9	**3a**	100/1/5	^{n}BuOH	50	53	48
10	**3a**	100/1/5	THF	50	0	
11[d]	**3a**	100/1/5	EtOH	50	quant.	47
12[e]	**4a**	100/1/0	EtOH	50	7	nd
13	**4a**	100/1/5	EtOH	50	99	42

[a]Standard procedure: catalyst and KO^{t}Bu (amounts given as S/C/B) were dissolved in ethanol (3 mL); acetophenone (50 mg, 48.5 μL, 0.416 mmol) was added, and the mixture was pressurized under H_2 for 16 h at 20 °C. [b]Determined by GC on a β-dex column. [c]The hydride complex was generated in situ by dissolving the corresponding dibromocarbonyl complex in THF (0.3 mL) and adding $NaBHEt_3$ (1 equiv). [d]PMe_3 (30 mol % vs catalyst) was added. [e]No base was added.

of **3a** is currently underway in our laboratory and will be published in due course.

As Yang[16] and Hopmann[17] have suggested that dihydride **4b** is the active species in ketone hydrogenation, we tested its chiral analogue **4a** as catalyst. No base was added to check whether **4a** is active per se (the function of the base is to activate the bromocarbonylhydrido complex **3a**). With other conditions remaining the same, the conversion of acetophenone was only 7% (entry 12). Addition of base restored catalytic activity and gave slightly lower enantioselectivity (entry 13).

Mechanistic Background. As mentioned in the Introduction, the mechanism of the direct hydrogenation of acetophenone with the achiral precatalyst [FeHBr(CO(**1b**)] (**3b**) in the presence of base has been thoroughly studied by DFT calculations.[15−17] As acetophenone is prostereogenic, the use of a chiral pincer ligand introduces additional information concerning the enantiodetermining step of the catalytic cycle, that is, the hydride transfer.[26−28] This may allow one to discriminate between the **D**, **I**, and **O** mechanisms (Scheme 9) suggested for **3b**, provided that they lead to significantly different enantioselectivity and/or different sense of induction. To clarify whether such a discrimination based on the absolute configuration of the product is possible, we performed DFT calculations on the enantiodetermining step of the hydrogenation of acetophenone with complex **3a** according to the three different mechanisms (Scheme 9). Before exposing our results, we summarize the main features of mechanisms **D**, **I**, and **O** for the achiral catalyst **3b**.

Mechanism **D** was initially suggested by Yang[16] and is based on the dihydride complex [FeH_2(CO)(**1b**)] (**4b**) (Scheme 1), which transfers a hydride to a noncoordinated acetophenone molecule. Hopmann has recently proposed a revised version that differs for the regeneration of the catalyst but not for the hydride transfer.[17] However, Milstein has shown that this dihydride does not react with acetophenone in a stoichiometric fashion.[15] As these findings strongly disfavor the involvement of dihydride in the catalytic cycle, Milstein considered alternative mechanisms. The classical inner-sphere Schrock−Osborne

DOI: 10.1021/acs.organomet.7b00816
Organometallics XXXX, XXX, XXX−XXX

Scheme 9. Enantiodetermining Step in Mechanisms D, I, and O

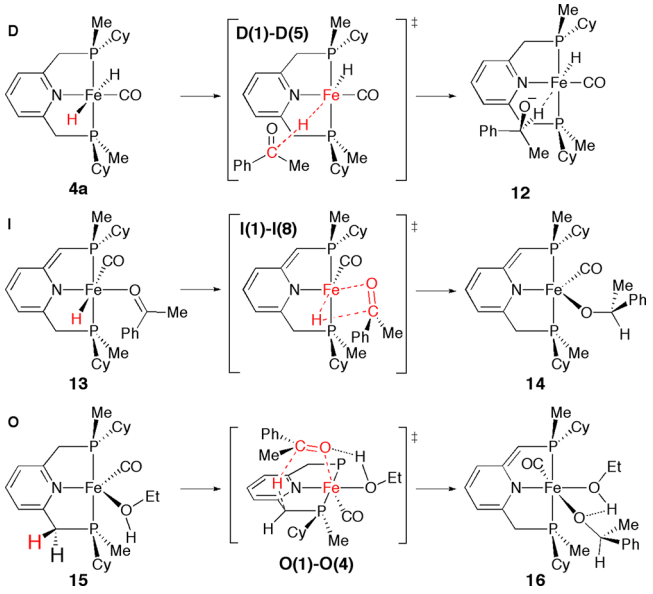

mechanism **I**[29−31] in which the C═O double bond of the coordinated ketone inserts into the Fe−H bond of monohydride **13** gave an unrealistically large energetic span (50.8 kcal mol^{-1}).[15] Therefore, an outer-sphere mechanism **O** was suggested that involves the Fe(0) complex **15**, from which a benzylic H atom of the PNP ligand is transferred as hydride to the carbonyl group of acetophenone. A hydrogen bond involving the coordinated ethanol molecule directs the incoming substrate and activates its carbonyl group toward nucleophilic attack,[11,15] which is reminiscent of the well-established bifunctional mechanism.[31,32] Based on the reasonable calculated energy span for **O** (21.7/24.5 kcal mol^{-1}) and on the lack of reactivity of dihydride [$FeH_2(CO)$(**1b**)] toward acetophenone, Milstein has concluded that **O** is the most probable mechanism.[15]

DFT Studies. The transition state (TS) structures and their relative free energies for mechanisms **D**, **I**, and **O** with the chiral pincer complex **3a** (Scheme 9) were studied by DFT. The TS structures previously optimized by Hopmann[17] for mechanism **D** and by Milstein[15] for mechanisms **I** and **O** were modified by introducing the cyclohexyl and methyl substituents on the P atoms. The phosphine fragments were taken from the X-ray structure of **2a**. Then, the structures were optimized for each TS (see Conformational Issues below and Supporting Information). The TSs and minima were calculated with the hybrid density functional B3LYP[33] with Grimme's D3BJ empirical correction for dispersion.[34] The SDD basis set with the associated Stuttgart-Dresden pseudopotential was used for Fe[35] and Dunning's basis set[36] with double-ζ for all other atoms. The solvent was described by the implicit polarizable continuum model.[37] Stationary points were characterized by vibrational analysis (only real frequencies for minima, one imaginary frequency for transition states), and intrinsic reaction coordinate (IRC) calculations were carried out on the transition states in order to confirm their correct identification. Computed harmonic frequencies were used to calculate the thermal contribution to Gibbs free energy at 298 K.

Conformational Issues. The X-ray structure of **2a** (Figure 1) shows that the five-membered rings P(1)−Fe−N(1)−C(2)−C(1) and P(2)−Fe−N(1)−C(3)−C(4) assume an envelope conformation with the P atom in the *endo* position and equatorial cyclohexyl groups. The conformational inversion of the ring swaps the cyclohexyl and methyl P-substituents between equatorial and axial positions and tilts the pyridine ring with respect to the P(1)−Fe−N(1) and P(2)−Fe−N(1) planes. Additionally, a five-membered chelate ring can also assume a planar conformation, which is energetically disfavored for cyclopentane.[38] The conformation of the five-membered chelate rings in the iron-bound PNP pincer ligand is described by the torsion angles P(1)−Fe−N(1)−C(2) (θ_1) and P(2)−Fe−N(1)−C(3) (θ_2) (Figure 2).

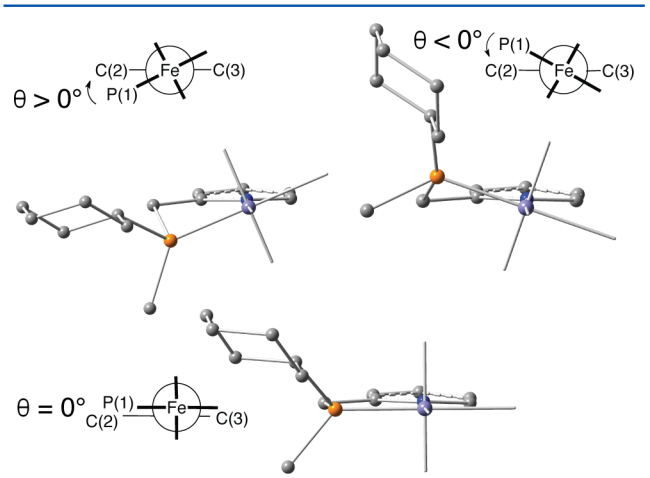

Figure 2. Conformation of the five-membered chelate ring (with Newman projection and dihedral angle θ).

The conformation of the chelate ring determines (a) whether the P-substituents are equatorial or axial in the envelope conformation, or inclinal in the planar one,[39] and (b) the tilt of the pyridine ring with respect to the P(1)−Fe−N(1) and P(2)−Fe−N(1) planes. In the dibromocarbonyl derivative **2a** (Figure 1), the chelate rings assume envelope conformations (θ_1 = 16°, θ_2 = 14°) with the P atom in the *endo* position. Positive θ values in the range of 12 to 27° give an envelope conformation in which the cyclohexyl group is equatorial. For negative θ values (−12 to −27°), the cyclohexyl group is axial. Dihedral angles θ close to 0° correspond to an inclinal cyclohexyl group. Largely different θ_1 and θ_2 angles tend to distort the P(1)−Fe−P(2) angle away from the ideal value of 180°. Therefore, the conformation of the chelate rings in the TSs **D**, **I**, and **O** (Scheme 9) was optimized by scanning $\theta_1 = \theta_2$ between −35 and 35° at 10° intervals (for a total of eight conformations). The resulting TSs are discussed below for the different mechanisms.

Dihydride Mechanism D. Mechanism **D** involves hydride transfer from dihydride complex **4a** to the noncoordinated acetophenone (Scheme 9).[16,17] The corresponding TSs (Figure 3) were modeled and optimized as described below.

The enantioface exposed to the hydride in the TS determines the absolute configuration of the alcohol, which is known from experiment. Overall, the structure of the transition states depends on (a) the enantioface of acetophenone, (b) the orientation of the substrate, and (c) the conformation of the pincer ligand. Initially, we studied the orientation of the substrate with the C═O bond of acetophenone parallel to the plane of the complex with a planar conformation of the pincer ligand.[40] The P(1)−Fe−C═O angle was scanned at 60°

DOI: 10.1021/acs.organomet.7b00816
Organometallics XXXX, XXX, XXX−XXX

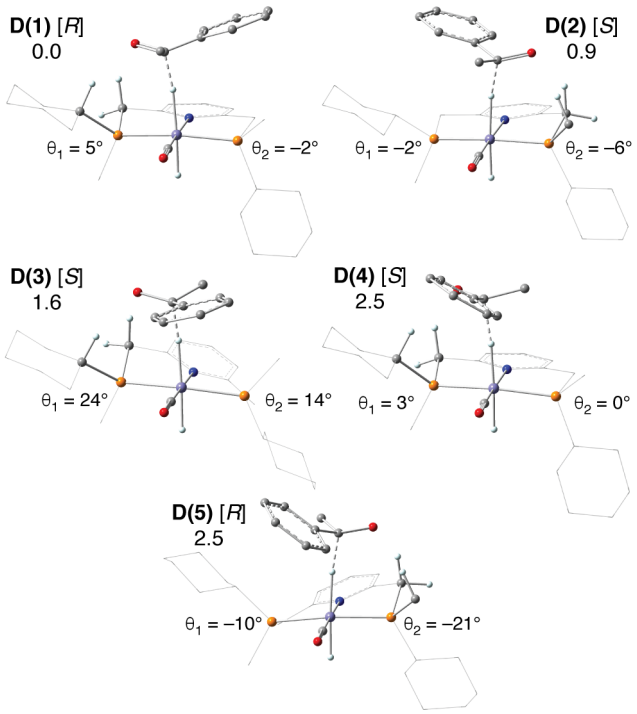

Figure 3. Transition states for the hydride transfer in mechanism **D**, torsion angles θ_1 and θ_2, and relative Gibbs free energies (in kcal mol^{-1}). Absolute configuration of 1-phenylethanol in brackets.

intervals (6 TSs) for the *R* and *S* enantiofaces of the acetophenone. For each enantioface, the resulting starting structures either did not converge or gave a single TS in which the oxygen atom of acetophenone is involved in two C−H···O interactions[41] with one of the two benzylic H atoms of the ligand and with the H atom on the *ipso* carbon of the adjacent methyl or cyclohexyl groups on the phosphine, in agreement with Hopmann's TSs.[17] In **D(1)**, the O atom of the carbonyl group is frozen between these two H atoms (O···H distances are 2.22 and 2.20 Å). Hence, for each enantioface, only one orientation of the substrate is possible (P(1)−Fe−C═O = −17° in **D1**, −155° in **D2**, Figure 3).

The C−H···O interaction between a benzylic H atom and the CO group forces the chelate rings to assume planar (**D(1)**, **D(2)**, **D(4)**) or partially flattened conformations (**D(3)** and **D(5)**, Figure 3), which are less stable than the envelope. In particular, the PNP pincer in **D(3)** (θ_1 = 24°, θ_2 = 14°) and **D(5)** (θ_1 = −10°, θ_2 = −21°) exhibits a highly distorted overall conformation.

In the low-energy TSs **D(1)** and **D(2)**, the phenyl ring of the acetophenone points toward the pyridine backbone. A closer analysis reveals that the phenyl group of the acetophenone forms a C−H···π interaction with the benzylic H atom (2.56 Å in **D(1)**, 2.58 Å in **D(2)**). The energetically lowest TS **D(1)** predicts the formation of (*R*)-1-phenylethanol, which is against experiment and strongly disfavors this mechanism. The next TS lies 0.9 kcal mol^{-1} higher in energy and would give the *S* enantiomer.

Inner-Sphere Mechanism I. For the achiral PNP pincer complex **3b**, Milstein has suggested that mechanism **I** involves a hydride ketone complex analogous to **13** (Scheme 9 and Figure 4). Intermediate **13**, which features a deprotonated benzylic position and dearomatized pyridine ring,[11,42] evolves toward the insertion of the C═O double bond into the Fe−H one

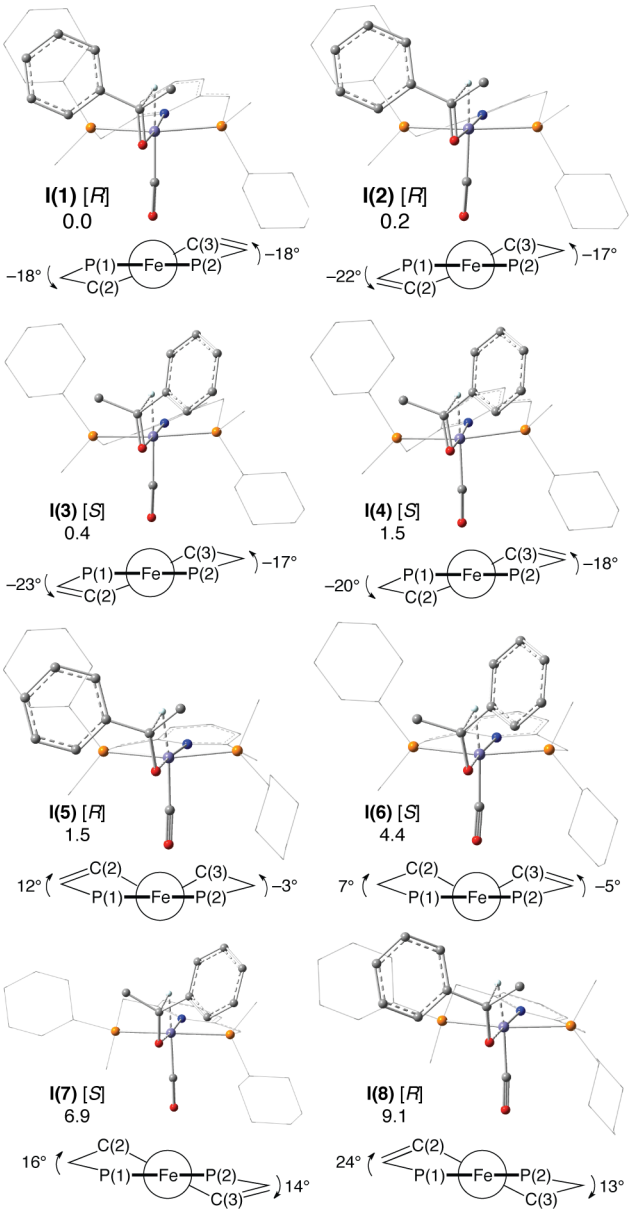

Figure 4. Transition states for the hydride transfer in mechanism **I**. The product stereochemistry is given in brackets. Relative Gibbs free energies are expressed in kcal mol^{-1}. Deprotonation sites and θ_1 (left) and θ_2 (right) values are given in the Newman projections.

according to a classical Schrock−Osborn mechanism.[31] The structure of the resulting transition states is determined by (a) the enantioface of acetophenone exposed to the catalyst, (b) the position of the deprotonated benzylic carbon, and (c) the conformation of the chelate rings (Figure 4).

The enantioface exposed in the TS determines the absolute configuration of the resulting alcohol, which is the experimental parameter. The relative orientation of the substrate is constrained by the coordination of the O atom to the metal center and by the interaction with the hydride. Concerning (b), either −CH_2− benzylic unit of the pyridine backbone can be deprotonated, as indicated by the Newman projections in Figure 4. As for point (c), the conformation of the chelate ring determines whether the cyclohexyl and methyl substituents on phosphorus are either axial or equatorial. Eight different conformations were scanned as explained above. The

DOI: 10.1021/acs.organomet.7b00816
Organometallics XXXX, XXX, XXX−XXX

optimization of these overall 32 structures converged to the eight TSs shown in Figure 4.

The four energetically lower optimized transition states **I(1)**–**I(4)** have envelope conformations with axial cyclohexyl substituents (the dihedral angles θ_1 and θ_2 are negative in the range between −23 and −17°). Transition state **I(5)** features an envelope conformation for the P(1)–Fe–N(1)–C(1)–C(2) ring (θ_1 = 12°), whereas the P(2)–Fe–N(1)–C(3)–C(4) ring is flattened with θ_2 close to zero, and the cyclohexyl group is inclinal. In **I(6)**, both chelate rings are planar (both θ_1 and θ_2 close to 0°) with inclinal cyclohexyl substituents. The last two transition states (**I7**–**I8**) show a positive value of the two dihedral angles between 13 and 24°, typical of the envelope conformation with equatorial cyclohexyl substituents.

Rather surprisingly, the four lowest-lying transition states **I(1)**–**I(4)** have at least one axial cyclohexyl group. A closer analysis reveals that the phenyl group of the acetophenone forms a C–H···π interaction with the H atom on the *ipso* carbon of the adjacent P-Cy group (2.34 Å in **I(1)**, 2.32 Å in **I(2)**). The P-Me group is involved in analogous but weaker interactions in **I(3)** and **I(4)** (2.57 and 2.50 Å, respectively). Eventually, the two lowest in energy transition states of the inner-sphere mechanism (**I(1)** and **I(2)**) predict the formation of (*R*)-1-phenylethanol, in contrast with the experimental results (48% ee (*S*)).

Outer-Sphere Mechanism O. In the enantiodetermining step of Milstein's unprecedented outer-sphere mechanism **O**,[15] a benzylic H atom of the ligand is transferred as hydride from the five-coordinate iron(0) complex [Fe(CO)(EtOH)(**1a**)] (**15**) to acetophenone (Scheme 9). Complex **15** exists as conformers **15a** and **15b**. Negative θ_1 and θ_2 torsion angles are indicative of axial cyclohexyl substituents such as in **15b**, **O(1)**, and **O(3)**. Positive θ torsion angles imply axial P-Me groups such as in **15a**, **O(2)**, and **O(4)** (Figure 5). The approach of acetophenone to **15a**/**15b** is directed by the incipient C═O···Fe interaction and by the C═O···HOEt hydrogen bond to coordinated ethanol. Two parameters determine the structure of the possible TSs, that is, (a) the prostereogenic face of acetophenone and (b) the benzylic position involved in the hydride transfer. The latter correlates to the conformation of the chelate rings: The benzylic H atom on the left points toward acetophenone only for θ > 0° (that is, for equatorial cyclohexyl groups, Figure 5 right).

The conformation of structures involving hydride transfer from the left benzylic methylene was optimized by scanning θ between 35 and 5° (see above) with both acetophenone enantiofaces. This optimization converged to the TSs (**O(2)** and **O(4)** in Figure 5). The same procedure was repeated with θ < 0° for transfer from the benzylic position on the right, which gave **O(1)** and **O(3)**. As acetophenone approaches **15a**/**15b**, the conformation of the chelate ring changes to allow the attack of the benzylic H atom as hydride onto the carbonyl C atom, as indicated by the small, but significant, increase in $|\theta|$ values (Figure 5).

An intriguing result is that the most stable TS **O(1)** features axial cyclohexyl groups and hence the less stable conformation. To find out how the conformation of **15a**/**15b** correlates with that of **O(1)**–**O(4)**, we performed an IRC analysis. The calculated reaction coordinates were found to connect **O(2)** and **O(4)** to **15a**, which has the same conformation (equatorial cyclohexyl groups) as the starting species (Figure 5, right). Analogously, **O(1)** and **O(3)** are linked to **15b**, both bearing axial cyclohexyl groups (Figure 5, left). Conformer **15a**, which bears equatorial cyclohexyl substituents, is more stable than **15b** by 0.4 kcal mol^{-1} (Figure 6).

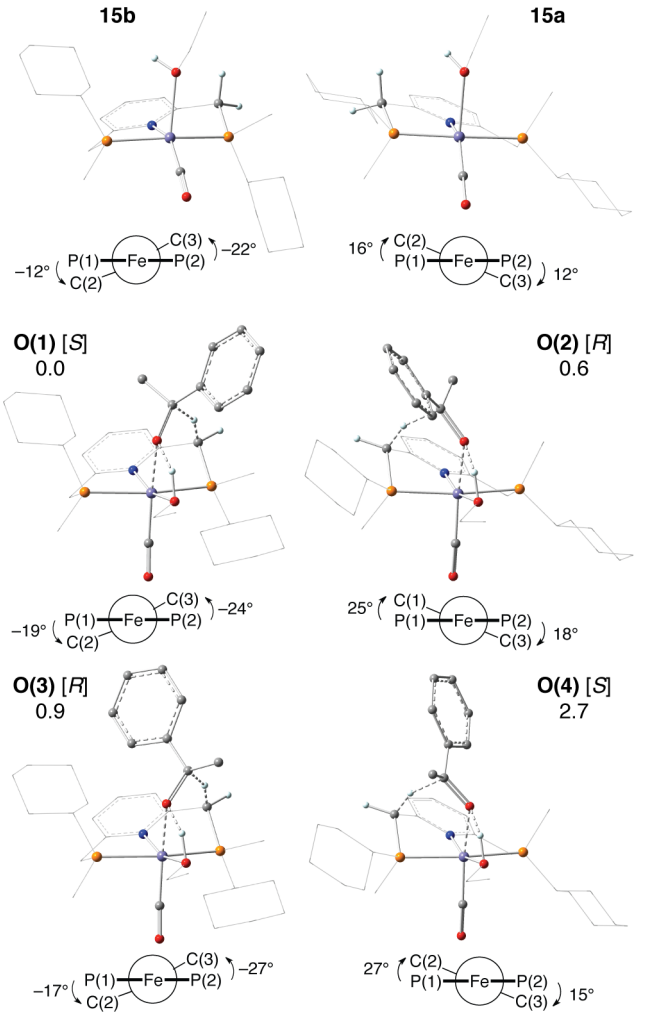

Figure 5. Iron(0) complexes **15a** and **15b** and transition states **O(1)**–**O(4)** for the hydride transfer in mechanism **O** with product stereochemistry in brackets. Newman projections give θ_1 (left) and θ_2 (right). Relative Gibbs free energies are expressed in kcal mol^{-1}.

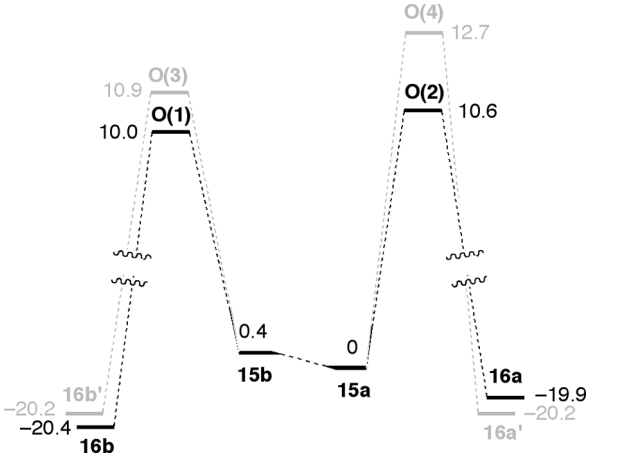

Figure 6. Computed reaction pathway for the hydride transfer in mechanism **O**. Relative Gibbs free energies are expressed in kcal mol^{-1}. The Gibbs free energies of **16** are not in scale.

DOI: 10.1021/acs.organomet.7b00816
Organometallics XXXX, XXX, XXX–XXX

No significant conformational changes were detected between **15a**/**15b** and the corresponding transition states. Therefore, we conclude that the inversion of the chelate rings occurs between the starting species **15a** and **15b**. We were unable to locate a transition state for their interconversion, which suggests that the energy hypersurface for the chelate ring flip is flat without large barriers. Accordingly, the pseudorotation of the five-membered ring in cyclopentane through the half-chair conformation has a time scale on the order of picoseconds or sub-picoseconds at room temperature.[43] For these reasons, we assume that the equilibrium between **15a** and **15b** is fast, and that they react under Curtin−Hammett conditions to give the 1-phenylethoxide complexes **16a**/**16a′** and **16b**/**16b′** (Scheme 9). This implies that the ratio of the products depends on the energy difference between the transition states.[44,45]

The above conclusion concerning the conformational equilibria is corroborated by a closer analysis of the four TSs. In **O(1)**, the benzylic C−H bond to the hydrogen atom that is being transferred as hydride is very weakly perturbed (1.23 Å), whereas the distance to the carbonyl C atom is as long as 1.68 Å. Both observations suggest an early transition state, in agreement with the Hammond−Leffler postulate for exergonic reactions such as hydride transfer.[46] Also, there is only little structural reorganization between **15** and **O(1)**−**O(4)**, as indicated by the minor changes in $|\theta|$ (Figure 5), which further supports the retention of conformation along the reaction coordinate.

Perusal of TSs **O(1)**−**O(4)** in Figure 5 suggests that their energy depends on the steric interactions of the phenyl ring of acetophenone (a) with the pincer backbone and (b) with the substituents on phosphorus, which depends on the conformation of the chelate rings. In the energetically low-lying TSs **O(1)** and **O(2)**, acetophenone directs the methyl group above the pyridine and phenyl in TSs **O(3)** and **O(4)**. For the P-substituents, acetophenone places the phenyl group toward the small P-Me group in **O(1)** and toward the large P-Cy group in **O(2)**, which is in qualitative agreement with **O(1)** being more stable. However, Figure 5 shows that there is no clear and easily predictable trend in the interactions between acetophenone the P-substituents in the case of **O(3)** and, in particular, of **O(4)**, whose high energy possibly mainly derives from the conformational strain (θ = 27°; see below).

H^-/H^+ Transfer. Each TS **O(1)**−**O(4)** shows a strong hydrogen bond between the H atom of the coordinated ethanol O−H and the oxygen atom of acetophenone. In **O(1)**, the C═O···HOEt distance is 1.50 Å. It has been shown previously[15] that this hydrogen bond directs and activates the incoming acetophenone toward hydride attack. In the case of mechanism **O**, we have studied the hydride transfer step by IRC profile analysis, which shows that TSs **O(1)**−**O(4)** evolve to four diastereomeric intermediates (**16a**, **16a′**, **16b**, and **16b′**; see Supporting Information) that contain coordinated 1-phenylethoxide involved in a strong hydrogen bond to the iron-bound ethanol. In **16b**, which derives from the lowest-energy TS **O(1)**, the hydrogen atom is still closer to ethoxide (1.02 Å) than to the oxygen atom of 1-phenylethanolate (1.58 Å), which implies that the transfers of hydride and proton are not concerted.

Although the possibility that H^+ transfer might be kinetically relevant appears remote, we studied the proton transfer step from ethanol to 1-phenylethanolate, which converts **16b** to **17b** (Figure 7). In the corresponding **TS(16b−17b)**, which was

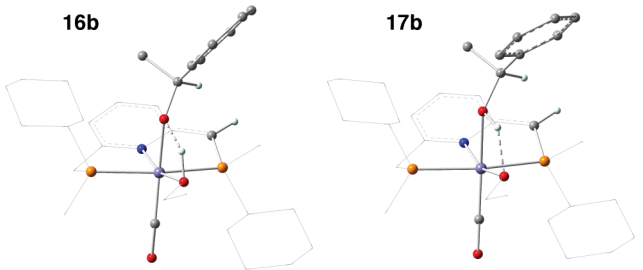

Figure 7. Complexes before (**16b**) and after (**17b**) the proton transfer in mechanism **O**.

located on the energy hypersurface, the proton is equidistant from the oxygen atoms of ethoxide (1.22 Å) and 1-phenylethanolate (1.20 Å). IRC analysis indicates that the reaction is without barrier (Figure S24). As the energy of **TS(16b−17b)** is much lower than that of **O(1)**, we conclude that only the preceding hydride transfer affects the enantioselectivity. In **17b**, the proton is located on the oxygen atom of 1-phenylethanol (1.01 Å) and is involved in a hydrogen bond with ethoxide (the O···H distance is 1.64 Å) (see Supporting Information). Hence, at difference with the achiral catalyst **3b**, for which concerted H^-/H^+ transfer occurs, the mechanism for **3a** is stepwise with consecutive hydride and proton transfers.[15]

Conformational Flexibility. Our DFT study highlights the pivotal role played by the changes of the ligand conformation in the different intermediates. Surprisingly, the conformation with axial cyclohexyl groups in the Fe(0) intermediate **15a**/**15b** is just 0.4 kcal mol^{-1} less stable than with equatorial cyclohexyls (Figure 6). To gain further insight into the flexibility of the PNP ligand **1a**, we applied the activation strain model (ASM) to transition states **O(1)**−**O(4)**.[47] The breakdown of the electronic energy $\Delta\Delta E^{\ddagger}_{tot}$ indicates that the interaction of the catalyst with acetophenone in the transition state ($\Delta\Delta E^{\ddagger}_{int}$) is less important than the distortion of the two reactants during their approach ($\Delta\Delta E^{\ddagger}_{strain}$) (Table 2). Compared to **O(1)**, a

Table 2. ASM Analysis of Transition States O(1)−O(4)[a,b]

	O(1)[S]	O(2)[R]	O(3)[R]	O(4)[S]
$\Delta\Delta E^{\ddagger}_{tot}$	0	0.7	1.6	3.6
$\Delta\Delta E^{\ddagger}_{int}$	0	−1.4	−3.0	−1.4
$\Delta\Delta E^{\ddagger}_{strain}$	0	2.1	4.6	5.0
$\Delta\Delta E^{\ddagger}_{strain/sub}$	0	−1.0	2.1	−0.2
$\Delta\Delta E^{\ddagger}_{strain/cat}$	0	3.1	2.5	5.2
$\lvert\Delta\theta\rvert$	2°	9°	5°	11°

[a]Relative electronic energies are expressed in kcal mol^{-1}. [b]For each TS, $|\Delta\theta| = |\theta(\mathbf{O}) - \theta(\mathbf{15})|$ refers to the conformation of the chelate ring involved in hydride transfer (see Figure 5).

significant deformation of acetophenone is observed only for **O(3)**. Thus, the major contribution to the strain energy $\Delta\Delta E^{\ddagger}_{strain}$ is the distortion of the catalyst, which is mainly due to the conformational change of the chelate ring involved in hydride transfer (Figure 5) and can be expressed as the increase of $|\theta|$ in the corresponding chelate ($|\Delta\theta|$, Table 2). The data in Table 2 show that TSs **O(1)** and **O(3)**, which relate to the less stable conformer **15b** bearing axial cyclohexyl groups, undergo less conformational rearrangement than **O(2)** and **O(4)**, which connect to the more stable **15a**. Accordingly, **O(1)** and **O(3)**

DOI: 10.1021/acs.organomet.7b00816
Organometallics XXXX, XXX, XXX−XXX

have the lowest $\Delta\Delta E^{\ddagger}_{strain/cat}$ values, which implies that **15b** has the best conformation for the approach of acetophenone.

Overall, the above DFT analysis suggests that the energy difference between different chelate ring conformations is small. In mechanism **D**, the most stable structures show a planar chelate ring, whereas the envelope conformation with axial cyclohexyl groups is the most stable for mechanism **I**. In mechanism **O**, the most stable transition state has envelope conformations with axial cyclohexyl groups, but the most stable starting minimum has envelope conformations with equatorial cyclohexyl groups, although the energies of the minima are very close. We conclude that PNP ligand **1a** is flexible and its conformation can be easily swapped by weak intermolecular interactions, such as the C−H···O bond in mechanism **D** and the C−H···π interaction in mechanisms **D** and **I**. In the same way, the steric hindrance significantly affects the relative conformation stability, as seen in mechanism **O**. Therefore, rigidifying the PNP backbone is the first priority in the attempt to achieve higher enantioselectivity.

Comparison of Mechanisms D, I, and O. Overall, the DFT study on the outer-sphere mechanism **O** indicates that the lowest energy transition state **O(1)** gives the alcohol with the *S* absolute configuration, which is in agreement with the experimental observation. The TSs responsible for the minor *R* enantiomer lie 0.6 and 0.9 kcal mol^{-1} higher than that leading to the *S* product. The Boltzmann distribution of the four transition states leads to 26% ee, which is in fair agreement with the experimentally observed enantioselectivity of 48% ee. The reaction profile for the reaction segment connecting the Fe(0) ethanol complex **15** to the Fe(II) 1-phenylethanol species **17** confirms that the hydride transfer step is kinetically competent. In contrast, the inner-sphere mechanism **I** predicts the wrong sense of induction, as the two lowest energy transition states lead to the *R* enantiomer instead of the experimentally observed *S* one.

Also dihydride mechanism **D** predicts the wrong *R* enantiomer. Additionally, Milstein observed that dihydride [FeH_2(CO)(**1b**)] (**4b**) does not react with acetophenone.[15] The chiral analogue [FeH_2(CO)(**1a**)] (**4a**) gives, at best, traces of 1-phenylethanol in the presence of acetophenone (1 equiv) after 24 h, which strongly disfavors its involvement in catalysis. We explain the residual activity (Table 1, entry 12) with the presence of unidentified catalytically active impurities, as suggested by the NMR spectra of **4a**. Upon addition of base (5 equiv), dihydride **4a** catalyzes the hydrogenation of acetophenone with similar conversion and enantioselectivity as **3a**. However, this does not lend support to dihydride mechanism **D**. In fact, the addition of base most probably triggers the deprotonation of the benzylic position of the PNP ligand. The resulting negatively charged and hence electron-rich dihydride might transfer hydride to acetophenone. The resulting five-coordinate hydridocarbonyl complex might undergo reductive elimination of H^+, reprotonation of the ligand, and EtOH coordination to form **15**, which is the catalytically active species of mechanism **O** (Scheme 9).

As a word of caution, though, we notice that our DFT studies do not categorically exclude mechanism **D** and, in particular, mechanism **I**, as the energy differences involved are small as compared to the accuracy of DFT methods. Still, the combined experimental and computational study on chiral catalyst **3a** supports Milstein's conclusion with its achiral analogue **3b** that the outer-sphere mechanism (**O**) is more likely than the dihydride (**D**) and inner-sphere one (**I**).[15] The importance of this result is that it is based on the experimentally observed sense of induction and is hence complementary to Milstein's considerations based on the calculated energetic span of the catalytic reaction.[15] Finally, we note that the discrimination of different mechanisms based on sense of induction and enantioselectivity is still a rare approach[48] and should be added to the toolbox of mechanistic investigation.

CONCLUSION

The C_2-symmetric enantiopure Fe-PNP dibromocarbonyl complex described herein directly transfers the highly successful, achiral pyridine-based Fe-PNP pincer chemistry to a closely related chiral analogue. The slightly altered reactivity and the structural differences in the solid state of the chiral analogue highlight the importance of the substituents at phosphorus in such systems.

Even more importantly, the DFT study on P-stereogenic **3a** discloses the pivotal role played by the conformation of the pincer ligand in the mechanism of enantioselection. The combination of stereogenic P donors with the 2,6-dimethylenepyridine backbone gives highly flexible complexes, which requires a thorough analysis and investigation of the conformational aspects. In particular, conformations in which the largest substituents occupy axial positions are easily stabilized by secondary interactions, which hampers simple, qualitative predictions of the relative stability of the transition states. We are currently investigating such aspects with related PNP ligands.

The P-stereogenic pincer **1a** gave a valuable contribution to the mechanistic debate concerning the catalytic hydrogenation of ketones with 2,6-dimethylenepyridine-based PNP pincer ligands. Indeed, Milstein's mechanism involving hydride transfer from the benzylic carbon of the ligand was the only one to reproduce the experimental sense of induction and enantioselectivity.

ASSOCIATED CONTENT

Supporting Information

The Supporting Information is available free of charge on the ACS Publications website at DOI: 10.1021/acs.organomet.7b00816.

Experimental procedures and characterization, X-ray crystallographic data for **2a**, and computational details (PDF)

Interactive structure (XYZ)

Accession Codes

CCDC 1584795 contains the supplementary crystallographic data for this paper. These data can be obtained free of charge via www.ccdc.cam.ac.uk/data_request/cif, or by emailing data_request@ccdc.cam.ac.uk, or by contacting The Cambridge Crystallographic Data Centre, 12 Union Road, Cambridge CB2 1EZ, UK; fax: +44 1223 336033.

AUTHOR INFORMATION

Corresponding Author

*E-mail: mezzetti@inorg.chem.ethz.ch.

ORCID

Antonio Mezzetti: 0000-0002-1824-7760

Notes

The authors declare no competing financial interest.

DOI: 10.1021/acs.organomet.7b00816
Organometallics XXXX, XXX, XXX−XXX

■ ACKNOWLEDGMENTS

This work was supported by SNF Grant 2-77063-16 and by ETH Grant 0-20356-17.

■ REFERENCES

(1) Casey, C. P.; Guan, H. *J. Am. Chem. Soc.* **2007**, *129*, 5816−5817.
(2) (a) Junge, K.; Schröder, K.; Beller, M. *Chem. Commun.* **2011**, *47*, 4849−4859. (b) Bauer, I.; Knölker, H.-J. *Chem. Rev.* **2015**, *115*, 3170−3387. (c) Darcel, C.; Sortais, J. B. *Top. Organomet. Chem.* **2015**, *50*, 173−216. (d) Ollevier, T.; Keipour, H. *Top. Organomet. Chem.* **2015**, *50*, 259−309. (e) Fürstner, A. *ACS Cent. Sci.* **2016**, *2*, 778−789.
(3) Magano, J.; Dunetz, J. R. *Org. Process Res. Dev.* **2012**, *16*, 1156−1184.
(4) Selected papers: (a) Sui-Seng, C.; Freutel, F.; Lough, A. J.; Morris, R. H. *Angew. Chem., Int. Ed.* **2008**, *47*, 940−943. (b) Mikhailine, A.; Lough, A. J.; Morris, R. H. *J. Am. Chem. Soc.* **2009**, *131*, 1394−1395. (c) Sonnenberg, J. F.; Coombs, N.; Dube, P. A.; Morris, R. H. *J. Am. Chem. Soc.* **2012**, *134*, 5893−5899. (d) Mikhailine, A. A.; Maishan, M. I.; Lough, A. J.; Morris, R. H. *J. Am. Chem. Soc.* **2012**, *134*, 12266−12280. (e) Zuo, W. W.; Lough, A. J.; Li, Y. F.; Morris, R. H. *Science* **2013**, *342*, 1080−1083. (f) Zuo, W. W.; Prokopchuk, D. E.; Lough, A. J.; Morris, R. H. *ACS Catal.* **2016**, *6*, 301−314.
(5) Li, Y. Y.; Yu, S. L.; Shen, W. Y.; Gao, J. X. *Acc. Chem. Res.* **2015**, *48*, 2587−2598.
(6) (a) Bigler, R.; Huber, R.; Mezzetti, A. *Angew. Chem., Int. Ed.* **2015**, *54*, 5171. (b) Bigler, R.; Mezzetti, A. *Org. Process Res. Dev.* **2016**, *20*, 253. (c) Bigler, R.; Huber, R.; Stöckli, M.; Mezzetti, A. *ACS Catal.* **2016**, *6*, 6455. (d) De Luca, L.; Mezzetti, A. *Angew. Chem., Int. Ed.* **2017**, *56*, 11949−11953.
(7) Fe(II) complexes containing tetradentate ligands only give slow H_2 activation: Morris, R. H. *Chem. Soc. Rev.* **2009**, *38*, 2282−2291.
(8) (a) Lagaditis, P. O.; Sues, P. E.; Sonnenberg, J. F.; Wan, K. Y.; Lough, A. J.; Morris, R. H. *J. Am. Chem. Soc.* **2014**, *136*, 1367−1380. (b) Zirakzadeh, A.; Kirchner, K.; Roller, A.; Stöger, B.; Widhalm, M.; Morris, R. H. *Organometallics* **2016**, *35*, 3781−3787. (c) Smith, S. A. M.; Lagaditis, P. O.; Lüpke, A.; Lough, A. J.; Morris, R. H. *Chem. - Eur. J.* **2017**, *23*, 7212−7216.
(9) Grabulosa, A. *P-Stereogenic Ligands in Enantioselective Catalysis*; RSC Catalysis Series No. 7; Royal Society of Chemistry: Cambridge, 2011.
(10) For a single example of a P-stereogenic pincer ligand used for the hydrogenation of ketones with Ru(II), see: Arenas, I.; Boutureira, O.; Matheu, M. I.; Díaz, Y.; Castillón, S. *Eur. J. Org. Chem.* **2015**, *2015*, 3666−3669.
(11) Langer, R.; Leitus, G.; Ben-David, Y.; Milstein, D. *Angew. Chem., Int. Ed.* **2011**, *50*, 2120−2124.
(12) Zell, T.; Ben-David, Y.; Milstein, D. *Angew. Chem., Int. Ed.* **2014**, *53*, 4685−4689.
(13) Zell, T.; Ben-David, Y.; Milstein, D. *Catal. Sci. Technol.* **2015**, *5*, 822−826.
(14) Garg, J. A.; Chakraborty, S.; Ben-David, Y.; Milstein, D. *Chem. Commun.* **2016**, *52*, 5285−5288.
(15) Langer, R.; Iron, M. A.; Konstantinovski, L.; Diskin-Posner, Y.; Leitus, G.; Ben-David, Y.; Milstein, D. *Chem. - Eur. J.* **2012**, *18*, 7196−7209.
(16) Yang, X. Z. *Inorg. Chem.* **2011**, *50*, 12836−12843.
(17) Morello, G. R.; Hopmann, K. H. *ACS Catal.* **2017**, *7*, 5847−5855.
(18) Kozuch, S.; Shaik, S. *Acc. Chem. Res.* **2011**, *44*, 101−110.
(19) Miura, T.; Yamada, H.; Kikuchi, S.-I.; Imamoto, T. *J. Org. Chem.* **2000**, *65*, 1877−1880.
(20) Muci, A. R.; Campos, K. R.; Evans, D. A. *J. Am. Chem. Soc.* **1995**, *117*, 9075−9076.
(21) Nagata, K.; Matsukawa, S.; Imamoto, T. *J. Org. Chem.* **2000**, *65*, 4185−4188.
(22) The optical purity of (*R*)-*tert*-butyl(hydroxymethyl)methylphosphine borane has been improved by crystallization of the benzoyl ester. See: Imamoto, T.; Sugita, K.; Yoshida, K. *J. Am. Chem. Soc.* **2005**, *127*, 11934−11935. With **7**, the benzoyl ester was a colorless oil at room temperature.
(23) McKinstry, L.; Livinghouse, T. *Tetrahedron* **1995**, *51*, 7655−7666.
(24) The common deboronation reaction with amines proceeds sluggishly with trialkyl phosphines. See: Lloyd-Jones, G. C.; Taylor, N. P. *Chem. - Eur. J.* **2015**, *21*, 5423−5428.
(25) Gorgas, N.; Stöger, B.; Veiros, L. F.; Pittenauer, E.; Allmaier, G.; Kirchner, K. *Organometallics* **2014**, *33*, 6905−6914.
(26) Dub, P. A.; Ikariya, T. *J. Am. Chem. Soc.* **2013**, *135*, 2604−2619.
(27) Li, L.; Pan, Y.; Lei, M. *Catal. Sci. Technol.* **2016**, *6*, 4450−4457.
(28) Sonnenberg, J. F.; Wan, K. Y.; Sues, P. E.; Morris, R. H. *ACS Catal.* **2017**, *7*, 316−326.
(29) Schrock, R. R.; Osborn, J. A. *J. Chem. Soc. D* **1970**, *9*, 567−568.
(30) Clapham, S. E.; Hadzovic, A.; Morris, R. H. *Coord. Chem. Rev.* **2004**, *248*, 2201−2237.
(31) Samec, J. S. M.; Bäckvall, J.-E.; Andersson, P. G.; Brandt, P. *Chem. Soc. Rev.* **2006**, *35*, 237−248.
(32) (a) Hashiguchi, S.; Fujii, A.; Takehara, J.; Ikariya, T.; Noyori, R. *J. Am. Chem. Soc.* **1995**, *117*, 7562−3. (b) Haack, K.-J.; Hashiguchi, S.; Fujii, A.; Ikariya, T.; Noyori, R. *Angew. Chem., Int. Ed. Engl.* **1997**, *36*, 285−288. (c) Noyori, R.; Yamakawa, M.; Hashiguchi, S. *J. Org. Chem.* **2001**, *66*, 7931−7944. (d) Ikariya, T.; Blacker, A. J. *Acc. Chem. Res.* **2007**, *40*, 1300−1308. (e) Dub, P. A.; Gordon, J. C. *ACS Catal.* **2017**, *7*, 6635−6655.
(33) Stephens, P. J.; Devlin, F. J.; Chabalowski, C. F.; Frisch, M. J. *J. Phys. Chem.* **1994**, *98*, 11623−11627.
(34) (a) Grimme, S.; Antony, J.; Ehrlich, S.; Krieg, H. *J. Chem. Phys.* **2010**, *132*, 154104−154119. (b) Grimme, S.; Ehrlich, S.; Goerigk, L. *J. Comput. Chem.* **2011**, *32*, 1456−1465.
(35) (a) Dolg, M.; Wedig, U.; Stoll, H.; Preuss, H. *J. Chem. Phys.* **1987**, *86*, 866−872. (b) Martin, J. M. L.; Sundermann, A. *J. Chem. Phys.* **2001**, *114*, 3408−3420.
(36) Dunning, T. H., Jr. *J. Chem. Phys.* **1989**, *90*, 1007−1023.
(37) (a) Tomasi, J.; Mennucci, B.; Cammi, R. *Chem. Rev.* **2005**, *105*, 2999−3093. (b) Cossi, M.; Scalmani, G.; Rega, N.; Barone, V. *J. Chem. Phys.* **2002**, *117*, 43−54.
(38) Saebø, S.; Cordell, F. R.; Boggs, J. E. *J. Mol. Struct.: THEOCHEM* **1983**, *104*, 221−232.
(39) Cremer, D. *Isr. J. Chem.* **1980**, *20*, 12−19.
(40) This conformation was chosen according to Hopmann's TS.[17]
(41) (a) Desiraju, G.; Steiner, T. *The Weak Hydrogen Bond*; Oxford University Press: Oxford, 1999. (b) Steiner, T. *Crystallogr. Rev.* **2003**, *9*, 177−228.
(42) (a) Ben-Ari, E.; Leitus, G.; Shimon, L. J. W.; Milstein, D. *J. Am. Chem. Soc.* **2006**, *128*, 15390−15391. (b) Zhang, J.; Leitus, G.; Ben-David, Y.; Milstein, D. *J. Am. Chem. Soc.* **2005**, *127*, 10840−10841. (c) Milstein, D. *Top. Catal.* **2010**, *53*, 915−923.
(43) (a) Kilpatrick, J. E.; Pitzer, K. S.; Spitzer, R. *J. Am. Chem. Soc.* **1947**, *69*, 2483−2485. (b) Bauman, L. E.; Laane, J. *J. Phys. Chem.* **1988**, *92*, 1040−1051. (c) Cui, W.; Li, F.; Allinger, N. L. *J. Am. Chem. Soc.* **1993**, *115*, 2943−2951. (d) Han, S. J.; Kang, Y. K. *J. Mol. Struct.: THEOCHEM* **1996**, *362*, 243−255. (e) Lightner, D. A.; Gurst, J. E. *Organic Conformation Analysis and Stereochemistry from Circular Dichroism Spectroscopy*; Wiley-VCH: New York, 2000. (f) Anslyn, E. V.; Dougherty, D. A. *Modern Physical Organic Chemistry*; University Science Books: Herdon, VA, 2005. (g) Ocola, E. J.; Bauman, L. E.; Laane, J. *J. Phys. Chem. A* **2011**, *115*, 6531−6542.
(44) Seeman, J. I. *Chem. Rev.* **1983**, *83*, 83−134.
(45) Curtin−Hammett conditions are assumed also for mechanisms **D** and **I** with regard to the conformational equilibrium and for **I** with respect to the protonation/deprotonation equilibrium at the benzylic positions.
(46) (a) Leffler, J. E. *Science* **1953**, *117*, 340−341. (b) Hammond, G. *J. Am. Chem. Soc.* **1955**, *77*, 334−338.
(47) Fernández, I.; Bickelhaupt, F. M. *Chem. Soc. Rev.* **2014**, *43*, 4953−4967.
(48) For a recent example, see: Santoro, S.; Liao, R.-Z.; Marcelli, T.; Hammar, P.; Himo, F. *J. Org. Chem.* **2015**, *80*, 2649−2660.

DOI: 10.1021/acs.organomet.7b00816
Organometallics XXXX, XXX, XXX−XXX